Confocal-Raman Microscopy Enables Label-Free, Quantitative, and Structurally-Informative Detection of DNA Hybridization at Porous Silica Surfaces

Grant J. Myres, Eric M. Peterson, and Joel M. Harris*
Department of Chemistry, University of Utah, 315 South 1400 East
Salt Lake City, UT 84112-0850 USA

Abstract

Characterization of DNA at solid/liquid interfaces remains a challenge because most surface sensitive techniques are unable to provide quantitative insight into base content, length, or structure. Surface-enhanced Raman scattering measurements of DNA hybridization at plasmonic-metal substrates has been used to overcome small Raman-scattering cross sections; however, SERS measurements are not generally quantitative, due to the fall-off in the scattering signal with the decay of the electric-field enhancement from the surface, which also limits the length of oligonucleotides that can be investigated. In this work, we introduce an experimental methodology in which confocal-Raman microscopy is used to characterize hybridization reactions of ssDNA immobilized at the solid/liquid interface of porous silica particles. By focusing the femtoliter confocal-probe volume within a single porous particle, signal enhancement arises from the ~1,500-times greater surface area compared to a planar substrate. Because the porous support is a purely dielectric material, the scattering signal is independent of the proximity of the oligonucleotide to the silica surface. With this technique, we characterize a 19-mer capture strand and determine its hybridization efficiency with 9-mer and 16-mer target sequences from the scattering of a structurally-insensitive phosphate-stretching mode. Changes in polarizability and frequency of scattering from DNA bases were observed that are consistent with Watson-Crick base-pairing. Quantification of base content from their duplex scattering intensities allows us to discriminate between hybridization of two target strands of equivalent length but with different recognition sequences. A duplex having a single-nucleotide polymorphism (SNP) could be distinguished from hybridization of a fully-complementary strand based on differences in base content and duplex conformation.

* Corresponding author: harrisj@chem.utah.edu

INTRODUCTION

Hybridization of target DNA sequences to complementary DNA probe strands, which are immobilized on solid supports, has been exploited for a wide variety of biotechnology and diagnostic applications.[1,2] Despite the many practical uses these hybridization assays performed at liquid-solid interfaces, most of our understanding of DNA hybridization derives from homogeneous solution-phase reactions. Far less information is available about hybridization at surfaces, where immobilized probe strands and their interactions with target strands in solution are susceptible to effects of surface electrostatics[3,4] and molecular crowding[5-7] that can modify conformations[4,8,9] and hybridization efficiency.[10] A major limitation in characterization of these interfacial reactions is that the surface densities of duplex oligonucleotides are small, in the range of 1-10 nmol/m^2, making detection of these interfacial reactions challenging. Incorporation of a fluorescent label into a target DNA strand allows very low densities of duplex formation events to be detected and quantified by means of single-molecule fluorescence imaging.[11-21] Fluorescence labeling has drawbacks, however, including the required ligation and purification of a labeled product and the influence that a label can have on the energetics and kinetics of hybridization.[22-25] Label-free fluorescence detection of DNA at surfaces is not practical because the room-temperature fluorescence quantum yields of DNA bases are vanishingly small, ~10^{-4}.[26] Label-free detection of hybridization at surfaces can be accomplished by surface-plasmon resonance[27-30] or micro-ring resonators,[31] which are sensitive to small changes in the interfacial refractive index that accompany duplex formation at immobilized DNA probes. While these label-free refractive-index detection methods are useful for biosensor applications, they do not report the base content or structure of the captured DNA, factors that are valuable in investigating interfacial hybridization reactions.

Vibrational spectroscopy has been shown to be a useful method for *in situ* characterization of interfacial DNA, having the potential to provide information on base content and structure. Sum-frequency generation (SFG), for example, has the sensitivity needed to detect monolayers of DNA at planar interfaces and yield insight into both molecular conformations and orientations of surface-bound oligonucleotides. [32,33] Because of limitations in frequency range however, SFG detection of DNA at surfaces has been limited to characterization of AT-rich sequences, making it less versatile for investigating hybridization reactions.[9,32-34] Attenuated-total-reflection infrared spectroscopy (ATR-FTIR) can access regions of the vibrational spectrum that contain information

related to all four bases.[35-37] Unfortunately, much of the infrared spectrum is obscured by strong absorption from water bands, and to date, FTIR surface investigations have been limited to qualitative rather than quantitative analysis of surface-bound oligonucleotide hybridization.[35,37,38]

Raman scattering exhibits a much smaller background from water than infrared absorption and has been used extensively to characterize oligonucleotide structure and reactions in free solution.[39-42] Because of small scattering cross sections ($\sigma \approx 10^{-28}$ cm^2) however, its application to surface-based hybridization has been limited. To extend Raman scattering measurements to analysis of DNA at interfaces, enhancement of scattering cross sections at plasmonic substrates has allowed surface-enhanced Raman spectroscopy (SERS) to characterize DNA at coinage-metal surfaces.[43-46] SERS has been used to investigate single-nucleotide polymorphisms,[45] relative base-composition,[45,46] secondary structure changes,[47-50] nucleic-acid derivatives,[45,51] and interactions between oligonucleotides and small molecules.[43,47] There are several drawbacks with SERS-based hybridization assays; selectivity can be a problem arising from non-specific interactions of DNA with typical plasmonic substrate surfaces.[43,44] Quantification with SERS is difficult because both the orientation of the oligonucleotide[49,52] and its distance from the plasmonic surface[44,53] significantly impact the observed band-intensities. The decay of the electric field enhancement with distance from the plasmonic surface complicates interpretation of data; it also limits the length of oligonucleotide that can be detected in a DNA-capture assay to around 9-bases or ~5 nm from the surface.[44] Due to these issues, SERS-based hybridization assays are generally limited to reporting qualitative information about interface composition of short oligonucleotides.[45,46]

Raman spectroscopy has potential to be an *in-situ* and structurally-informative method to characterize DNA hybridization at liquid-solid interfaces; however, an alternative approach is needed to overcoming the small scattering cross-sections that limit sensitivity for detecting surface populations of DNA. In this work, we report a method to immobilize capture-DNA strands on the interior surfaces of nanoporous silica gel particles. Using confocal-Raman microscopy, we focus *within an individual particle* and characterize the compositions of single-stranded probe DNA immobilized on the interior silica surfaces, along with duplexes formed by capturing target strands from solution. We overcome sensitive limitations of Raman scattering through significant *enhancement of surface area* that can be sampled within a particle.[54] In the several femtoliter confocal probe volume in the particle,[55,56] we interrogate ~1,500-times greater surface area compared to focusing the laser spot on a planar surface. Because the substrate is a purely dielectric

material and the internal surfaces of nanoporous structure are oriented randomly within the sampled probe volume, the scattering signal is independent of both orientation and proximity of the oligonucleotide relative to the silica surface. Using this methodology, we test its utility as a platform for quantitative analysis of DNA hybridization of probe strands immobilized at a silica surface. We evaluate non-specific interactions that might give rise to a background response, and we test the efficiency of capture by measuring scattering from phosphate vibrations, which are unaffected by duplex formation, for quantification. We observe polarizability and frequency changes of DNA vibrational modes that vary upon hybridization, providing insight into conformations adopted by the immobilized probe DNA as it forms an ordered duplex via Watson-Crick base-pairing. We also evaluate spectra for information about base-content and oligonucleotide conformations to detect single-nucleotide polymorphisms (SNPs) and to discern differences in the hybridization of oligonucleotides of equivalent length but with different recognition sequences.

EXPERIMENTAL SECTION

Reagents and Materials. Spherical chromatographic silica particles were obtained from YMC America (YMC Sil, Allentown, PA), with an average particle diameter of 10 μm, a pore diameter of 26 nm, and a specific surface area of 136 m^2/g, specified by the manufacturer. The silane reagent, 2,2-dimethoxy-1-thia-2-silacyclopentane, was purchased from Gelest (Morrisville, PA). DNA was prepared with solid-phase oligonucleotide synthesis (Table S1, Supporting Information) by the University of Utah HSC Core DNA Synthesis Facility. The 5'-maleimide-modifier phosphoramidite was purchased from Glen Research, (Maravai LifeSciences, San Diego, CA). Water used in all experiments was filtered using a Barnstead GenPure UV water purification system (ThermoFisher, Waltham, MA) and had a minimum resistivity of 18.0 MΩ·cm. N-phenylmaleimide 99%, sodium chloride (NaCl), dichloromethane (DCM), sulfuric acid, hydrogen peroxide and sodium phosphate dibasic heptahydrate ($Na_2HPO_4 \cdot 7H_2O$) were all purchased from Sigma-Aldrich (St. Louis, MO).

Thiol surface functionalization. A 50-mg sample of particles were first washed with acid piranha solution (60:40 concentrated sulfuric acid:30% hydrogen peroxide; *caution: corrosive, strong oxidizer, can react explosively with organics*) followed by twice rinsing in water and then ethanol followed by 5-times rinsing in anhydrous DCM. To achieve consistent sub-monolayer

coverages of surface thiol, 1.2 µL of 2,2-dimethoxy-1-thia-2-silacyclopentane was first diluted into 45 mL of DCM and mixed thoroughly. The clean particles were suspended in 5-mL of dry DCM and mixed with the 2,2-dimethoxy-1-thia-2-silacyclopentane in DCM, and allowed to react for 2 hours. Particles were then centrifuged and rinsed twice in ethanol followed by three-times in water. Particles were stored in deionized water at 2°C; surface immobilized thiols were stable over months (monitored by confocal Raman microscopy).

Preparation and surface immobilization of ssDNA. A retro Diels-Alder deprotection of the maleimide-conjugated to the DNA was performed by heating the sample in anhydrous toluene at 90°C for 4 hours. Toluene was pipetted off and the excess was evaporated at room temperature under 200-mTorr vacuum for 2 hours. The deprotected DNA was then suspended in water and filtered with a 3kD cutoff centrifugation filter. The sample was then diluted into 200-µL of pure deionized water for a stock solution concentration of ~1-mM 19-mer probe strand. For surface immobilization of ssDNA, a solution was prepared with a volume ratio of 1:1:2 DNA stock:1-mg/ml thiol particle:100-mM phosphate buffer with 300-mM NaCl. Samples were allowed to react overnight and were rinsed and spun down three times to remove excess ssDNA.

Microliter Sample Cells. To reduce the effects of sample evaporation of microliter sample aliquots, a simple cell comprising two coverslips and a double-stick gasket was developed. A paper punch was used to make a ~0.5”-diameter hole in a 125-µm thick double-stick tape (3M 9495MP). The backing paper was pealed, and the adhesive-exposed tape was laminated on a 22x22-mm No. 1.5 glass coverslip (Thermo Scientific), a 3-µL sample was pipetted directly in the middle of the exposed glass to ensure the aliquot didn’t come into contact with the double-stick tape which contained a contaminant that produced a fluorescent background. The second paper backing was then removed and a second coverslip was placed over the adhesive leaving the aliquot sandwiched between the two coverslips held together by double-stick tape.

Hybridization Experiments. All hybridization experiment were performed in 10-mM PBS buffer (pH 7.4). Samples of particles functionalized with the 19-mer probe strand were equilibrated with 5-µM concentrations of target strand batch-wise for ~12 hours to ensure hybridization equilibrium was achieved. Following equilibration with target strands, individual particles were characterized with the target strand simultaneously present in the sample. The 5-µM concentrations of solution target strand produced no detectable background.

Confocal Raman Microscopy. The confocal Raman microscope has been previously described in detail elsewhere.[54] Briefly, the 647.1-nm beam from a Kr^+ laser (Innova 90, Coherent Int., Santa Clara, CA) was first passed through a narrow band-pass filter followed by a 4X beam expander (50-25-4x-647, Special Optics Inc., Wharton, NJ) and reflected off of a dichroic mirror, and the 130-mW beam was directed into a 1.4 NA, 100X oil-immersion objective (CFL PLAN APO, Nikon Inc., El Segundo, CA), which produces a ~600-nm diameter beam waist at the focal plane. Light scattered from the confocal probe volume was collected by the same objective, transmitted through the dichroic mirror, passed through a 660 nm long-pass filter and focused through 50-μm slit of a 500-mm focal length spectrograph (Bruker 500IS) with a 300-line/mm diffraction grating blazed at 750 nm. Diffracted light is then displayed onto a charged coupled device (CCD) detector (Andor iDus 420, Andor USA, South Windsor, CT).

To collect spectra, the beam was initially focused at the coverslip/solution interface and translated upward in the z-dimension until silica particles adsorbed to the coverslip appear in the field of view. The stage was then adjusted in the x and y dimensions until the confocal probe volume was directed within an individual particle. Each spectrum reported represented the average of 3-min integrations collected from 12 different individual particles. This averaged the 6.5% particle-to-particle variation and avoided a photo-induced loss of immobilized DNA which could be detected after a 5-min exposure. Collected spectra were truncated to the spectral region of interest and baseline corrected with a rolling-circle algorithm.[57] All data analysis was carried out in Matlab (Mathworks, Natick, MA) using custom scripts. Unless specified, spectra are not normalized.

RESULTS AND DISCUSSION

***In-situ* characterization of the steps to immobilize DNA to silica surfaces.** Thiol-maleimide 'click' chemistry was chosen as the conjugation technique for the current work because the reaction is highly specific and has favorable reaction kinetics.[58] Additionally, maleimides can be conjugated to ssDNA in solid-phase synthesis, and the thiol-maleimide Michael addition reaction occurs spontaneously in mild aqueous solution conditions (0.1 M phosphate buffer pH 7.4). [59] There is a challenge in achieving homogeneous, fractional monolayer coverages of a surface thiol especially with traditional trialkoxysilanes reagents like (3-mercaptopropyl)-

trimethoxysilane, which are susceptible to cross-linking and subsequent growth of siloxane polymers from the surface.[60]

To ensure a controlled, reproducible, and homogeneous density of surface thiols to immobilize ssDNA, we employ a cyclic 5-membered-ring thia-silane reagent (2,2-dimethoxy-1-thia-2-silacyclopentane) for thiol surface immobilization.[59] Surface modification proceeds spontaneously as an efficient ring-opening reaction with surface silanol groups in organic solvents, resulting in the formation of a monomeric siloxane bond with the surface, where the dry conditions inhibit hydrolysis and polymerization of the methoxy-silane groups (Figure 1).[59] For surface functionalization, a sample of cleaned silica particles were reacted with a low concentration (160 µM) of 2,2-dimethoxy-1-thia-2-silacyclopentane in anhydrous DCM for 2 hours to limit the surface coverage. Raman spectra of the silica following functionalization is accompanied with the appearance of the 2580 cm^{-1} S-H stretching mode indicative of the presence of surface immobilized thiol (Figure 1). To quantify the surface coverage of the bound silane reagent, the total intensity of scattering from the C-H stretching modes of the immobilized silane was used for calibration through comparison with scattering from a commercial propyl-nitrile-derivatized silica having a previously-determined ligand surface density and specific surface area.[61] Using this means of surface characterization, we estimate our thiol surface density to be 180 ± 20 nmol/m^2 or about 5% of a full monolayer.

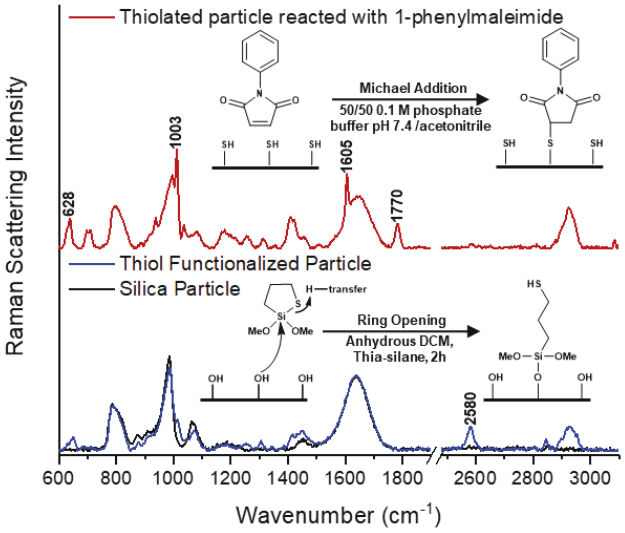

Figure 1. *In-situ* monitoring of silica surface derivatization. Bottom: bare silica (black) reacted with 2,2-dimethoxy-1-thia-2-silacyclopentane (blue). Top: thiolated silica reacted with 1-phenylmaleimide (red).

To investigate the reactivity of the surface thiol toward maleimide conjugation, thiolated particles were reacted with 100 µM 1-phenylmaleimide in 50/50 (v/v) acetonitrile/0.1 M phosphate buffer pH 7.4. Following 30-min of reaction, particle samples were washed by centrifugation three times with buffer. As can be observed in Figure 1, the significant loss of the 2580 cm^{-1} S-H stretching intensity is accompanied by the growth of the 628 cm^{-1} C-S stretch, 1003 cm^{-1} trigonal ring stretch, 1605 cm^{-1} C=C stretch and 1770 cm^{-1} succinimide stretch consistent with

efficient conversion of surface thiols to thiosuccinimides following equilibration with 1-phenylmaleimide.

Selective immobilization of maleimide-terminated probe DNA. To immobilize single-stranded DNA to the thiolated silica surface, a phosphate-buffer solution containing ~250-μM 19-mer DNA probe strand having a maleimide group at the 5'-end was reacted with thiolated silica particles for ~12-hours, and the unbound DNA was rinsed from the sample prior to characterization. The Raman spectrum of the silica particles with immobilized DNA is compared to the thiolated silica particles in Figure 2. A feature in the Raman spectrum that is consistent with surface immobilization of the probe DNA is the 1770 cm^{-1} succinimide stretching mode. A difference spectrum plotted in the figure clearly shows the Raman scattering bands associated with the surface-bound DNA probe, where the DNA bands labeled in the figure are assigned in Table S1 based on previous studies the literature.[39,40,42,62] The difference spectrum also compares favorably with the solution spectrum of the 19-mer probe strand (Figure S1). To test the selectivity of surface immobilization of maleimide–conjugated DNA, a 16-mer oligonucleotide without the reactive maleimide group ~500-μM in buffer was equilibrated with thiolated particles for ~12-hours. Following an equivalent rinse as above, no detectable spectral features indicative of the presence of DNA were observed (Figure S2) indicating no detectable non-specific interactions of ssDNA with thiolated particles.

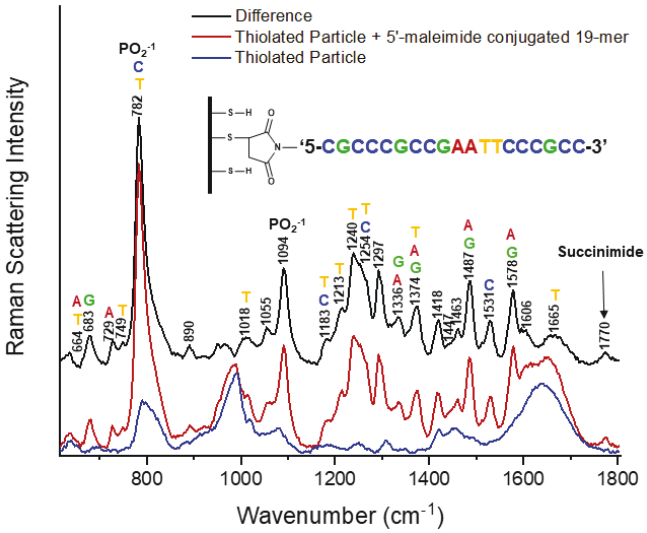

Figure 2. Immobilization of ssDNA by thiol-maleimide conjugation. Thiolated silica particle (blue) reacted with 5'-maleimide conjugated ssDNA (red); the difference spectrum (black) highlights ssDNA and succinimide modes.

To estimate the DNA surface coverage, the scattering intensity of the succinimide band (1770 cm^{-1}) in the surface-immobilized DNA sample (Figure 2) was compared to that from the particles reacted with 1-phenylmaleimide Figure 1, whose surface density was quantified above. The results indicate that the DNA coverage is 21 ± 2% of the monolayer formed with 1-phenylmaleimide, or a surface density of ssDNA of 38 ± 6 nmol/m^2. Previous reports have indicated that hybridization efficiency of surface-immobilized DNA can be inhibited by surface-

crowding or steric effects at coverages exceeding ~50nmol/m^2. We would therefore anticipate efficient hybridization of the immobilized-probe strand with target strands from solution. The particle-to-particle reproducibility of surface coverage was also assessed by measuring the Raman scattering from 10 individual DNA-derivatized particles. The Raman scattering from the more intense DNA bands in the spectra exhibit a relative standard deviation of ~6.5%, which is comparable to the baseline noise (Figure S3). This reproducibility represents absolute particle-to-particle variation in signal, because these spectra were not normalized to their total intensity or to a specific band. Based on the surface coverage result above, the amount of DNA immobilized within a single probed particle is quite small, ~2.6 fmol; nevertheless, the local concentration within the particle, ~2.6 mM, is sufficient to generate easily-detected Raman scattering.

Selective hybridization of immobilized ssDNA. To investigate the reactivity and selectivity of the immobilized 19-mer capture strand, a solution containing 5-μM 16-mer complement was equilibrated with the 19-mer oligonucleotide conjugated particles. As shown in Figure 3, equilibration is accompanied by spectral changes consistent with duplex formation. While polarizabilities of many nucleotide vibrational modes (Table S1) are sensitive to Watson-Crick base pairing,[40] scattering from the 1094 cm^{-1} phosphate stretching mode has been previously shown to be insensitive to DNA hybridization, conformation, and base-composition.[40] Comparing the scattering from the

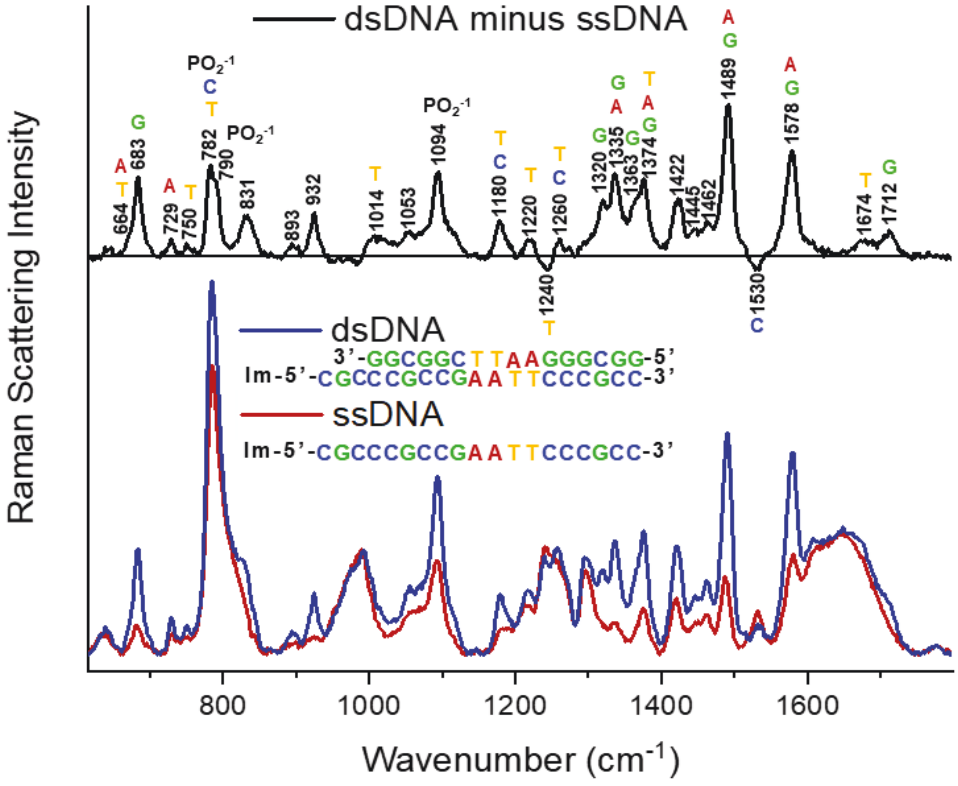

Figure 3. Raman spectra of immobilized 19-mer capture strand before (red) and following equilibration with 5 μM 16-mer target strand (blue). Spectral changes due to hybridization are observed in the difference spectrum (black).

immobilized 19-mer single-stranded probe and its duplex with the 16-mer complement (correcting for the differences in the number of DNA bases), we find that the capture efficiency of the 19-mer probe is 1.1 ± 0.1, indistinguishable from 100% capture efficiency. This result is in good agreement with SPR hybridization efficiency at planar surfaces[10,30] (at equivalent surface densities) meaning that the curvature of the porous silica surface does not inhibit accessibility or activity of surface immobilized oligonucleotides. The selectivity of capture was tested using a 9-mer non-complementary target strand, where no detectable changes in the Raman spectrum relative to the 19-mer probe strand were observed (Figure S4); note that reaction with 9-mer complementary target strands produces easily-detected duplex scattering (see next section).

In addition to observing unit capture efficiency, both band frequencies (Table S1.) and changes in band intensities highlighted in the difference spectrum provide information about the conformation of the surface immobilized DNA. For example, the 1240 cm^{-1} thymine ring stretching mode is sensitive to the effects of base-stacking, and its polarizability has been previously reported to decrease substantially following duplex-formation.[41] As can be observed in the difference spectrum, the thymine ring stretch has a negative intensity although following hybridization the abundance of thymine localized at the surface doubles. In addition, the 1532 cm^{-1} cytosine stretching mode is also observed to decreases in intensity following hybridization making it an additional reporter of base-pairing.[40]

Certain modes also exhibit frequencies that are sensitive to both DNA handedness and base-content, because of torsional stress on the DNA-backbone. For example, the frequency of the PO_2^{-1} stretch varies from 745 – 807 cm^{-1} and is sensitive to DNA handedness. In the current work, we observe the PO_2^{-1} stretch at 790 cm^{-1}, a frequency characteristic of B-DNA. Additionally, the 831 cm^{-1} PO_2^{-1} shoulder apparent in the difference spectrum is only present in B-DNA; this mode appears over a 14 cm^{-1} range centered at 835 cm^{-1} and is informative of base-content.[42] In G-C rich dsDNA shifts towards 830 cm^{-1} whereas us A-T rich dsDNA, it shifts towards 840 cm^{-1}. In our current work, we observe a peak centered at 831 cm^{-1} consistent with the predominant G-C content (75%) of the immobilized duplex. Additionally, we observe shifting of the 1418 cm^{-1} C2'H_2 deformation band to 1422 cm^{-1} following duplex formation which is also consistent with the structure of B-DNA.[42]

Nucleotide band frequencies are also telling of DNA secondary structure. The guanine ring stretch for example is sensitive to duplex DNA handedness and secondary structural conformations

with bands appearing over a wide, 60 cm^{-1} frequency range centered at ~650 cm^{-1}.[39] The 683 cm^{-1} guanine stretch observed in the current work highlighted in the difference spectrum is indicative of the C2'-*endo/anti* conformer, which further confirms the presence of surface-immobilized duplex B-DNA.[39,42]

Hybridization of oligonucleotides of different length. To test our ability to distinguish between the hybridization of complementary strands of different length and base content, we equilibrate 19-mer capture strands with 9-mer and 16-mer complements. The spectra in Figure 4 demonstrate the capability of discerning between the hybridization of these respective sequences. Because scattering from the 1094 cm^{-1} phosphate stretching mode is insensitive to DNA hybridization, conformation, and base-composition,[40] we examine whether this intensity can reveal the absolute number of nucleotides. Plotting the intensity of the 1094 cm^{-1} phosphate stretching versus number of nucleotides for the single-capture strand, and 9-mer and 16-mer duplexes (19, 28 and 35) shows a linear relationship with no intercept, indicating that this scattering is proportional the total interfacial nucleotide content.

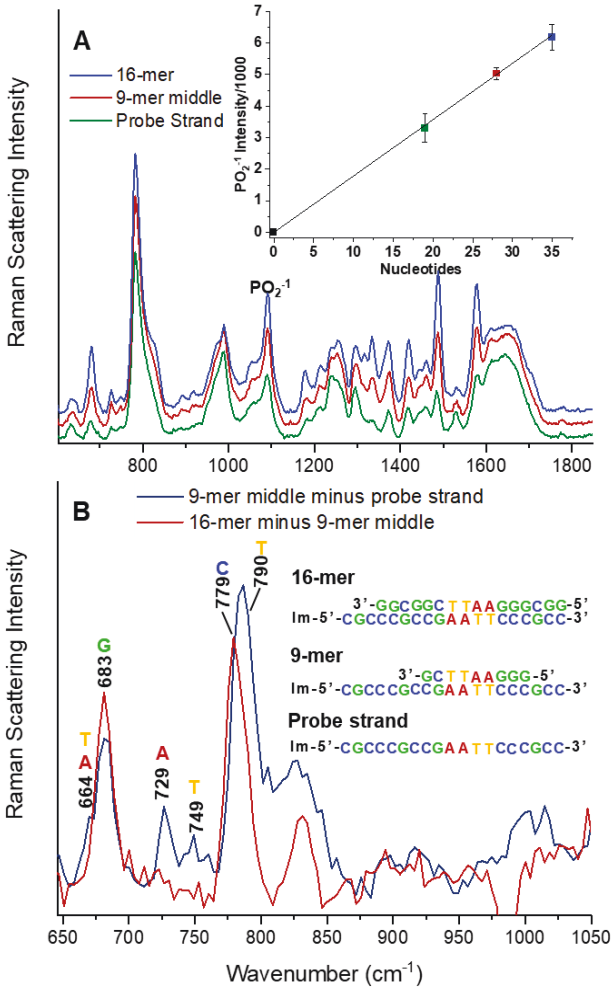

Figure 4. (A) Raman spectra of immobilized probe strand and hybridized 9-mer and 16-mer target strands: inset shows that phosphate intensity (1094 cm^{-1}) versus # of nucleotides is linear with a zero intercept. (B) Raman difference spectra (A) reveal quantitative base-content (see text).

Quantification of base composition, however, is more challenging because both the polarizability and frequency of base vibrational modes are sensitive to primary sequence and conformation. One means of gaining insight into the base-content of a fragment target sequence is by using both the 19-mer immobilize probe strand and 16-mer hybridized duplex as standards (Figure 4B). Subtraction of the 19-mer probe strand from the hybridized 9-mer duplex cancels the residual single-strand component in the 9-mer duplex, leaving only the spectral changes in forming the 9-mer duplex, including changes in intensity and frequency due to changes

in the probe strand conformation. Subtraction of the 9-mer duplex from the 16-mer duplex cancels overlapping double-strand component, leaving the non-overlapping regions of the 16-mer and residual intensity differences, as a consequence of capture strand conformation changes. This method of intensity isolation allows us to compare the base contributions of a fragment strand with the full complement spanning the entire immobilized probe strand.

From this analysis, we can detect that adenine (729 cm^{-1}) and thymine (749 cm^{-1}) content contributed by the 9-mer overlaps with the 16-mer as indicated by the non-zero intensity in the (9-mer minus probe strand) spectrum (Figure 4B, blue) and zero intensity in the (16-mer minus 9-mer) spectrum (Figure B, red). The intensities of the guanine mode at 683 cm^{-1} in Figure 4B provide quantitative information about the G-content of the two target strands. The guanine intensity in the (16-mer minus 9-mer) spectrum (red) is 24 ± 2% greater than the guanine intensity in the (9-mer minus probe strand) spectrum (blue). Because the 9-mer sequence adds 4-guanine nucleotides to the probe DNA in forming a duplex, the ~25% greater guanine intensity in the (16-mer minus 9-mer) difference spectrum indicates that the 16-mer target contains 5-more guanine nucleotides than the 9-mer sequence, which is consistent with their structures.

Distinguishing the hybridization of two complement stands of equivalent length. Although oligonucleotides of different length or significantly different base content can be differentiated by their melting temperatures, a challenging measurement is to discern between two target oligonucleotides of equivalent length and similar base content that recognize different regions of an immobilized capture strand. This is challenging because the duplexes formed by two such target DNA strands would have similar stability and melting temperatures. More importantly, DNA melting temperatures or other measures of duplex stability do not reveal the base-composition of the captured target strands.

To address challenge, we tested whether differences in base content would be reflected in the spectra of duplexes formed by hybridization of two 9-mer DNA strands having the same length but

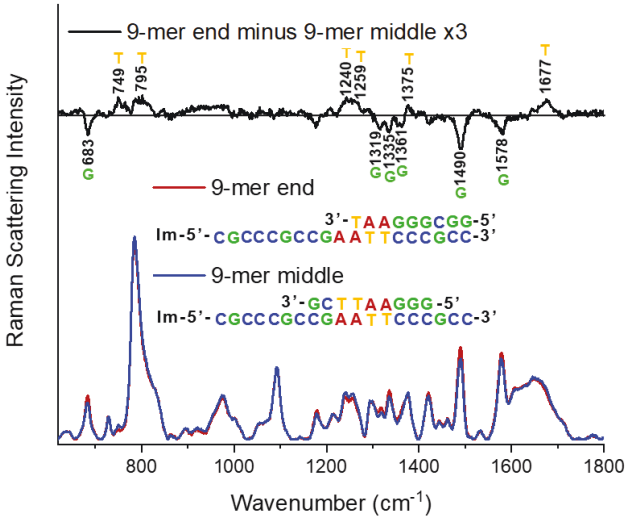

Figure 5. Distinguishing hybridization of two oligonucleotides of equivalent length that recognize different regions of a 19-mer immobilized capture sequence. Hybridized 9-mer middle (blue), 9-mer top (red), and a difference spectrum (top) that shows differences in base-content (black).

which target different regions of a 19-mer immobilized probe strand. We compare the Raman spectra of duplexes formed from two equivalent length 9-mer strands whose composition differs by a *single* thymine and guanine base and whose sequences are complementary to different regions of the 19-mer probe. The spectra normalized to the intensity of the 1094 cm^{-1} phosphate stretching mode (Figure 5) appear to be nearly identical. However, a difference spectrum produced by subtracting the spectra of the two duplexes shows that the two strands have equivalent adenine and cytosine content (no differences in scattering) but differ in their thymine and guanine content, which is evident in the respective positive and negative scattering intensities (Figure 5 top).

Detecting a single-nucleotide polymorphism. For diagnosis of certain genetic diseases, abnormality in primary sequence often results in a single-nucleotide polymorphism, where a change in a single base along the sequence must be detected.[63] In efforts to increase efficiency of SNP detection, label-free SPR and ring-resonator hybridization assays have been demonstrated to be capable of high-throughput analysis of mismatched sequences.[30,31,64] Unfortunately, these assays do not directly report changes in the target strand base-content or duplex structure and conformation. Here we test the sensitivity of interfacial Raman scattering from a DNA duplex to substitution of a single-mismatched base in an otherwise fully complementary 16-mer sequence.

Raman spectra normalized to the 1094 cm^{-1} phosphate stretching intensity of the duplexes formed with the fully complementary 16-mer strand and with a SNP containing a single adenine-thymine substitution are compared in Figure 6. While the individual spectra appear to be nearly identical, the difference spectrum reveals loss of adenine intensity in the negative-going bands at 1299, 1342, and 1580 cm^{-1}.[41] There is also a slight gain in thymine scattering intensity at 1240 and 1365 cm^{-1}. The most interesting feature in the difference spectrum is a shift of the 790 cm^{-1} thymine band to lower frequency 777 cm^{-1}. This shift in frequency is consistent with a change in the sugar-base conformation from the C2'-*endo/anti*

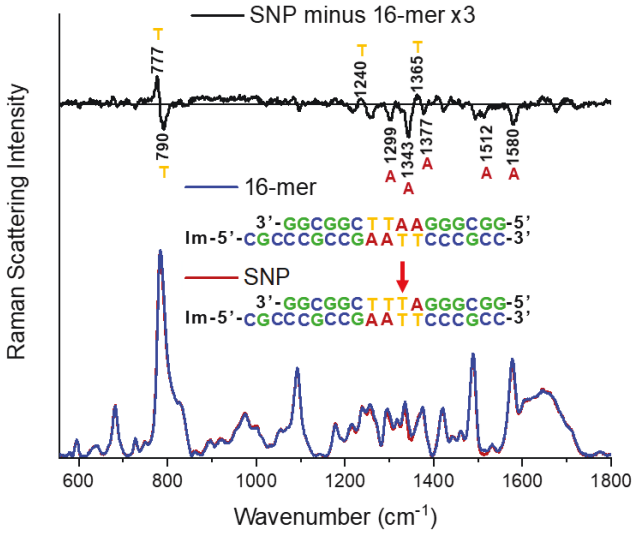

Figure 6. Detection of a single-nucleotide polymorphism. Hybridization of SNP sequence (red) and 16-mer complement (blue), difference spectrum showing changes in base content and conformation of the two the target strands (black).

conformer typical of B-form duplex DNA to the C3'-*endo/anti* conformer.[42] This disruption in sugar structure is consistent with previous accounts of a transversion mismatch adopting a wobble conformation[65,66] (Figure 6). Thus, the difference Raman spectrum comparing the scattering from the SNP and fully-complementary duplexes indicates a loss of adenine content, a gain in thymine, and a structural change at the SNP site, which relate to the respective sequences of the two target strands.

Conclusions and future applications. In this work, we have developed a new label-free approach to detecting and characterizing the reactions of surface-immobilized DNA probe strands reacting with target DNA from solution using confocal Raman microscopy. The enhanced surface area that can be probed within porous silica particles have enabled us to perform quantitative analysis of DNA hybridization. The reproducibility of the measurement and its independence of surface proximity or orientation allows us to quantify absolute oligonucleotide length while also gaining insight into base-content of captured target strands. We have demonstrated the utility of this method in detecting both a single-nucleotide polymorphism and distinguishing between target strands of different sequence and equivalent length with single-base sensitivity.

Future applications of this methodology will allow label-free measurements of association constants for the hybridization of target DNA with immobilized probes, thereby avoiding the significant impact that fluorescent labels have on the kinetics and stability of DNA duplexes.[23,25] This technology can detect not only immobilized single-stranded DNA and hybridized DNA targets, but also molecules that interact with double-stranded DNA. This capability will allow the association of small-molecule and peptide-based drugs that can modulate gene expression [67,68] to be investigated without labels. In addition to possible drug screening, binding constants can be determined along with their sequence-specific interactions that impact the stability and structure of dsDNA. These measurements would not be possible in homogeneous solution because of the inability to control excess drug concentrations at clinically-relevant nM levels when reacting with mM-concentration solutions of DNA required for detection. Localization of the capture dsDNA within an *individual porous particle* allows nM concentrations in the surrounding solution to supply the needed drug to reach equilibrium without depleting the solution concentration. This methodology can also be used for label-free structural investigation of proteins that bind to DNA including transcription factors, repair enzymes, and histones.[69-71] Finally, the association of immobilized DNA aptamers with small quantities of unlabeled protein targets can also be

measured, which could be useful in screening applications and in providing insight into structure-function relationships that lead to selectivity in DNA-aptamer biosensors.[72] To our knowledge, there is no other vibrational spectroscopy method currently capable of *in-situ,* quantitative and structurally-informative investigations of these interfacial oligonucleotide interactions.

ASSOCIATED CONTENT

Supporting Information.

Additional information on the oligonucleotide sequences, Raman band assignments, comparison of solution-phase and immobilized DNA, tests of non-specific DNA interactions with the thiolated silica surface, characterization of measurement reproducibility, and non-complementary control experiments.

ACKNOWLEDGEMENTS

This work was supported by the National Science Foundation under Grant CHE-1904424. The authors are grateful to Mike Hansen of the University of Utah Core DNA Synthesis Facility for contributions to this project. The authors also acknowledge informative conversations with Andrew Roberts and Emily Kirkeby on bioconjugation chemistry.

LITERATURE CITED

(1) Schneider, A.-K.; Niemeyer, C.M. DNA Surface Technology: From Gene Sensors to Integrated Systems for Life and Materials Sciences. *Angew. Chem. Int. Ed.* **2018**, *57*, 16959-16967.

(2) Sassolas, A.; Leca-Bouvier, B.D.; Blum, L.J. DNA Biosensors and Microarrays. *Chem. Rev.* **2008**, *108*, 109-139.

(3) Watkins, H.M.; Vallée-Bélisle, A.; Ricci, F.; Makarov, D.E.; Plaxco, K.W. Entropic and Electrostatic Effects on the Folding Free Energy of a Surface-Attached Biomolecule: An Experimental and Theoretical Study. *J. Am. Chem. Soc.* **2012**, *134*, 2120-2126.

(4) Watkins, H.M.; Ricci, F.; Plaxco, K.W. Experimental Measurement of Surface Charge Effects on the Stability of a Surface-Bound Biopolymer. *Langmuir* **2018**, *34*, 14993-14999.

(5) Watterson, J.H.; Piunno, P.A.E.; Wust, C.C.; Krull, U.J. Effects of Oligonucleotide Immobilization Density on Selectivity of Quantitative Transduction of Hybridization of Immobilized DNA. *Langmuir* **2000**, *16*, 4984-4992.

(6) Watkins, H.M.; Simon, A.J.; Ricci, F.; Plaxco, K.W. Effects of Crowding on the Stability of a Surface-Tethered Biopolymer: An Experimental Study of Folding in a Highly Crowded Regime. *J. Am. Chem. Soc.* **2014**, *136*, 8923-8927.

(7) Lei, Q.-l.; Ren, C.-l.; Su, X.-h.; Ma, Y.-q. Crowding-induced Cooperativity in DNA Surface Hybridization. *Sci. Rep.* **2015**, *5*, 9217.

(8) Howell, C.; Schmidt, R.; Kurz, V.; Koelsch, P. Sum-frequency-generation spectroscopy of DNA films in air and aqueous environments. *Biointerphases* **2008**, *3*, FC47-51.

(9) Ho, J.-J.; Skoff, D.R.; Ghosh, A.; Zanni, M.T. Structural Characterization of Single-Stranded DNA Monolayers Using Two-Dimensional Sum Frequency Generation Spectroscopy. *J. Phys. Chem. B* **2015**, *119*, 10586-10596.

(10) Peterson, A.W. The effect of surface probe density on DNA hybridization. *Nucleic Acids Res.* **2001**, *29*, 5163-5168.

(11) Jungmann, R.; Steinhauer, C.; Scheible, M.; Kuzyk, A.; Tinnefeld, P.; Simmel, F.C. Single-Molecule Kinetics and Super-Resolution Microscopy by Fluorescence Imaging of Transient Binding on DNA Origami. *Nano Lett.* **2010**, *10*, 4756-4761.

(12) Kastantin, M.; Schwartz, D.K. Connecting Rare DNA Conformations and Surface Dynamics Using Single-Molecule Resonance Energy Transfer. *ACS Nano* **2011**, *5*, 9861-9869.

(13) Dupuis, Nicholas F.; Holmstrom, Erik D.; Nesbitt, David J. Single-Molecule Kinetics Reveal Cation-Promoted DNA Duplex Formation Through Ordering of Single-Stranded Helices. *Biophys. J.* **2013**, *105*, 756-766.

(14) Kastantin, M.; Schwartz, D.K. DNA Hairpin Stabilization on a Hydrophobic Surface. *Small* **2013**, *9*, 933-941.

(15) Monserud, J.H.; Schwartz, D.K. Mechanisms of Surface-Mediated DNA Hybridization. *ACS Nano* **2014**, *8*, 4488-4499.

(16) Johnson-Buck, A.; Su, X.; Giraldez, M.D.; Zhao, M.; Tewari, M.; Walter, N.G. Kinetic fingerprinting to identify and count single nucleic acids. *Nat. Biotechnol.* **2015**, *33*, 730-732.

(17) Sobek, J.; Rehrauer, H.; Schauer, S.; Fischer, D.; Patrignani, A.; Landgraf, S.; Korlach, J.; Schlapbach, R. Single-molecule DNA hybridisation studied by using a modified DNA sequencer: a comparison with surface plasmon resonance data. *Methods Appl. Fluoresc.* **2016**, *4*, 015002.

(18) Su, X.; Li, L.; Wang, S.; Hao, D.; Wang, L.; Yu, C. Single-Molecule Counting of Point Mutations by Transient DNA Binding. *Sci. Rep.* **2017**, *7*, 43824.

(19) Yazawa, K.; Furusawa, H. Probing Multiple Binding Modes of DNA Hybridization: A Comparison between Single-Molecule Observations and Ensemble Measurements. *ACS Omega* **2018**, *3*, 2084-2092.

(20) Chen, J.; Bremauntz, A.; Kisley, L.; Shuang, B.; Landes, C.F. Super-Resolution mbPAINT for Optical Localization of Single-Stranded DNA. *ACS Appl. Mater. Interfaces* **2013**, *5*, 9338-9343.

(21) Peterson, E.M.; Manhart, M.W.; Harris, J.M. Single-Molecule Fluorescence Imaging of Interfacial DNA Hybridization Kinetics at Selective Capture Surfaces. *Anal. Chem.* **2016**, *88*, 1345-1354.

(22) Moreira, B.G.; You, Y.; Owczarzy, R. Cy3 and Cy5 dyes attached to oligonucleotide terminus stabilize DNA duplexes: Predictive thermodynamic model. *Biophys. Chem.* **2015**, *198*, 36-44.

(23) Peterson, E.M.; Manhart, M.W.; Harris, J.M. Competitive Assays of Label-Free DNA Hybridization with Single-Molecule Fluorescence Imaging Detection. *Anal. Chem.* **2016**, *88*, 6410-6417.

(24) Morrison, L.E.; Stols, L.M. Sensitive fluorescence-based thermodynamic and kinetic measurements of DNA hybridization in solution. *Biochemistry* **1993**, *32*, 3095-3104.

(25) Peterson, E.M.; Reece, E.J.; Li, W.; Harris, J.M. Super-Resolution Imaging of Competitive Unlabeled DNA Hybridization Reveals the Influence of Fluorescent Labels on Duplex Formation and Dissociation Kinetics. *J. Phys. Chem. B* **2019**, *123*, 10746-10756.

(26) Callis, P.R. Electronic States and Luminescence of Nucleic Acid Systems. *Annu. Rev. Phys. Chem.* **1983**, *34*, 329-357.

(27) Thiel, A.J.; Frutos, A.G.; Jordan, C.E.; Corn, R.M.; Smith, L.M. In Situ Surface Plasmon Resonance Imaging Detection of DNA Hybridization to Oligonucleotide Arrays on Gold Surfaces. *Anal. Chem.* **1997**, *69*, 4948-4956.

(28) Peterlinz, K.A.; Georgiadis, R.M.; Herne, T.M.; Tarlov, M.J. Observation of Hybridization and Dehybridization of Thiol-Tethered DNA Using Two-Color Surface Plasmon Resonance Spectroscopy. *J. Am. Chem. Soc.* **1997**, *119*, 3401-3402.

(29) Nelson, B.P.; Grimsrud, T.E.; Liles, M.R.; Goodman, R.M.; Corn, R.M. Surface Plasmon Resonance Imaging Measurements of DNA and RNA Hybridization Adsorption onto DNA Microarrays. *Anal. Chem.* **2000**, *73*, 1-7.

(30) Peterson, A.W.; Wolf, L.K.; Georgiadis, R.M. Hybridization of Mismatched or Partially Matched DNA at Surfaces. *J. Am. Chem. Soc.* **2002**, *124*, 14601-14607.

(31) Qavi, A.J.; Mysz, T.M.; Bailey, R.C. Isothermal Discrimination of Single-Nucleotide Polymorphisms via Real-Time Kinetic Desorption and Label-Free Detection of DNA Using Silicon Photonic Microring Resonator Arrays. *Anal. Chem.* **2011**, *83*, 6827-6833.

(32) Stokes, G.Y.; Gibbs-Davis, J.M.; Boman, F.C.; Stepp, B.R.; Condie, A.G.; Nguyen, S.T.; Geiger, F.M. Making "Sense" of DNA. *J. Am. Chem. Soc.* **2007**, *129*, 7492-7493.

(33) Li, Z.; Weeraman, C.N.; Azam, M.S.; Osman, E.; Gibbs-Davis, J.M. The thermal reorganization of DNA immobilized at the silica/buffer interface: a vibrational sum frequency generation investigation. *Phys. Chem. Chem. Phys.* **2015**, *17*, 12452-12457.

(34) Walter, S.R.; Geiger, F.M. DNA on Stage: Showcasing Oligonucleotides at Surfaces and Interfaces with Second Harmonic and Vibrational Sum Frequency Generation. *J. Phys. Chem. Lett.* **2010**, *1*, 9-15.

(35) Brewer, S.H.; Anthireya, S.J.; Lappi, S.E.; Drapcho, D.L.; Franzen, S. Detection of DNA Hybridization on Gold Surfaces by Polarization Modulation Infrared Reflection Absorption Spectroscopy. *Langmuir* **2002**, *18*, 4460-4464.

(36) Saprigin, A.V.; Thomas, C.W.; Dulcey, C.S.; Patterson, C.H.; Spector, M.S. Spectroscopic quantification of covalently immobilized oligonucleotides. *Surf. Interface Anal.* **2005**, *37*, 24-32.

(37) Riccardi, C.S.; Hess, D.W.; Mizaikoff, B. Surface-modified ZnSe waveguides for label-free infrared attenuated total reflection detection of DNA hybridization. *Analyst* **2011**, *136*, 4906.

(38) Tanaka, K.; Hirano-Iwata, A.; Miyamoto, K.-I.; Kimura, Y.; Niwano, M. In situSurface Infrared Study of DNA Hybridization on Au Island Films Evaporated on Silicon Surfaces. *Japanese Journal of Applied Physics* **2009**, *48*, 04C186.

(39) Benevides, J.M.; Thomas, G.J. Characterization of DNA structures by Raman spectroscopy: high-salt and low-salt forms of double helical poly(dG-dC) in H2O and D2O solutions and application to B, Z and A-DNA*. *Nucleic Acids Research* **1983**, *11*, 5747-5761.

(40) Duguid, J.G.; Bloomfield, V.A.; Benevides, J.M.; Thomas, G.J., Jr. DNA melting investigated by differential scanning calorimetry and Raman spectroscopy. *Biophys. J.* **1996**, *71*, 3350-3360.

(41) Movileanu, L.; Benevides, J.M.; Thomas, G.J. Temperature dependence of the raman spectrum of DNA. II. Raman signatures of premelting and melting transitions of poly(dA)·poly(dT) and comparison with poly(dA-dT)·poly(dA-dT)*. **2002**, *63*, 181-194.

(42) Benevides, J.M.; Overman, S.A.; Thomas, G.J. Raman, polarized Raman and ultraviolet resonance Raman spectroscopy of nucleic acids and their complexes. *J. Raman Spectrosc.* **2005**, *36*, 279-299.

(43) Barhoumi, A.; Zhang, D.; Tam, F.; Halas, N.J. Surface-Enhanced Raman Spectroscopy of DNA. *J. Am. Chem. Soc.* **2008**, *130*, 5523-5529.

(44) Marotta, N.E.; Beavers, K.R.; Bottomley, L.A. Limitations of Surface Enhanced Raman Scattering in Sensing DNA Hybridization Demonstrated by Label-Free DNA Oligos as Molecular Rulers of Distance-Dependent Enhancement. *Anal. Chem.* **2013**, *85*, 1440-1446.

(45) Guerrini, L.; Krpetić, Ž.; Van Lierop, D.; Alvarez-Puebla, R.A.; Graham, D. Direct Surface-Enhanced Raman Scattering Analysis of DNA Duplexes. *Angew. Chem.* **2015**, *127*, 1160-1164.

(46) Xu, L.-J.; Lei, Z.-C.; Li, J.; Zong, C.; Yang, C.J.; Ren, B. Label-Free Surface-Enhanced Raman Spectroscopy Detection of DNA with Single-Base Sensitivity. *J. Am. Chem. Soc.* **2015**, *137*, 5149-5154.

(47) Neumann, O.; Zhang, D.; Tam, F.; Lal, S.; Wittung-Stafshede, P.; Halas, N.J. Direct Optical Detection of Aptamer Conformational Changes Induced by Target Molecules. *Anal. Chem.* **2009**, *81*, 10002-10006.

(48) Li, Y.; Han, X.; Zhou, S.; Yan, Y.; Xiang, X.; Zhao, B.; Guo, X. Structural Features of DNA G-Quadruplexes Revealed by Surface-Enhanced Raman Spectroscopy. *J. Phys. Chem. Lett.* **2018**, *9*, 3245-3252.

(49) Rusciano, G.; De Luca, A.C.; Pesce, G.; Sasso, A.; Oliviero, G.; Amato, J.; Borbone, N.; D'Errico, S.; Piccialli, V.; Piccialli, G.; Mayol, L. Label-Free Probing of G-Quadruplex Formation by Surface-Enhanced Raman Scattering. *Anal. Chem.* **2011**, *83*, 6849-6855.

(50) Li, Y.; Gao, T.; Xu, G.; Xiang, X.; Han, X.; Zhao, B.; Guo, X. Base-Pair Contents and Sequences of DNA Double Helices Differentiated by Surface-Enhanced Raman Spectroscopy. *J. Phys. Chem. Lett.* **2019**, *10*, 3013-3018.

(51) Barhoumi, A.; Halas, N.J. Label-Free Detection of DNA Hybridization Using Surface Enhanced Raman Spectroscopy. *J. Am. Chem. Soc.* **2010**, *132*, 12792-12793.

(52) Barhoumi, A.; Zhang, D.; Halas, N.J. Correlation of Molecular Orientation and Packing Density in a dsDNA Self-Assembled Monolayer Observable with Surface-Enhanced Raman Spectroscopy. *J. Am. Chem. Soc.* **2008**, *130*, 14040-14041.

(53) Singh, A.K.; Khan, S.A.; Fan, Z.; Demeritte, T.; Senapati, D.; Kanchanapally, R.; Ray, P.C. Development of a Long-Range Surface-Enhanced Raman Spectroscopy Ruler. *J. Am. Chem. Soc.* **2012**, *134*, 8662-8669.

(54) Kitt, J.P.; Harris, J.M. Confocal Raman Microscopy for in Situ Detection of Solid-Phase Extraction of Pyrene into Single C18–Silica Particles. *Anal. Chem.* **2014**, *86*, 1719-1725.

(55) Korzeniewski, C.; Kitt, J.P.; Bukola, S.; Creager, S.E.; Minteer, S.D.; Harris, J.M. Single Layer Graphene for Estimation of Axial Spatial Resolution in Confocal Raman Microscopy Depth Profiling. *Anal. Chem.* **2019**, *91*, 1049-1055.

(56) Bridges, T.E.; Houlne, M.P.; Harris, J.M. Spatially Resolved Analysis of Small Particles by Confocal Raman Microscopy: Depth Profiling and Optical Trapping. *Anal. Chem.* **2004**, *76*, 576-584.

(57) Brandt, N.N.; Brovko, O.O.; Chikishev, A.Y.; Paraschuk, O.D. Optimization of the Rolling-Circle Filter for Raman Background Subtraction. *Appl. Spectrosc.* **2006**, *60*, 288-293.

(58) Saito, F.; Noda, H.; Bode, J.W. Critical Evaluation and Rate Constants of Chemoselective Ligation Reactions for Stoichiometric Conjugations in Water. *ACS Chem. Biol.* **2015**, *10*, 1026-1033.

(59) Kim, D.; Zuidema, J.M.; Kang, J.; Pan, Y.; Wu, L.; Warther, D.; Arkles, B.; Sailor, M.J. Facile Surface Modification of Hydroxylated Silicon Nanostructures Using Heterocyclic Silanes. *J. Am. Chem. Soc.* **2016**, *138*, 15106-15109.

(60) Mondin, G.; Lohe, M.R.; Wisser, F.M.; Grothe, J.; Mohamed-Noriega, N.; Leifert, A.; Dörfler, S.; Bachmatiuk, A.; Rümmeli, M.H.; Kaskel, S. Electroless copper deposition on (3-mercaptopropyl)triethoxysilane-coated silica and alumina nanoparticles. *Electrochim. Acta* **2013**, *114*, 521-526.

(61) Bryce, D.A.; Kitt, J.P.; Myres, G.J.; Harris, J.M. Confocal Raman Microscopy Investigation of Phospholipid Monolayers Deposited on Nitrile-Modified Surfaces in Porous Silica Particles. *Langmuir* **2020**, *36*, 4071-4079.

(62) Movileanu, L.; Benevides, J.M.; Thomas, G.J. Temperature dependence of the Raman spectrum of DNA. II. Raman signatures of premelting and melting transitions of poly(dA)·poly(dT) and comparison with poly(dA-dT)·poly(dA-dT)*. *Biopolymers* **2002**, *63*, 181-194.

(63) Wang, D.G. Large-Scale Identification, Mapping, and Genotyping of Single-Nucleotide Polymorphisms in the Human Genome. *Science* **1998**, *280*, 1077-1082.

(64) Li, Y.; Wark, A.W.; Lee, H.J.; Corn, R.M. Single-Nucleotide Polymorphism Genotyping by Nanoparticle-Enhanced Surface Plasmon Resonance Imaging Measurements of Surface Ligation Reactions. *Anal. Chem.* **2006**, *78*, 3158-3164.

(65) Batra, Vinod K.; Beard, William A.; Pedersen, Lars C.; Wilson, Samuel H. Structures of DNA Polymerase Mispaired DNA Termini Transitioning to Pre-catalytic Complexes Support an Induced-Fit Fidelity Mechanism. *Structure* **2016**, *24*, 1863-1875.

(66) Johnson, S.J.; Beese, L.S. Structures of Mismatch Replication Errors Observed in a DNA Polymerase. *Cell* **2004**, *116*, 803-816.

(67) Dervan, P.B. Molecular recognition of DNA by small molecules. *Biorg. Med. Chem.* **2001**, *9*, 2215-2235.

(68) Hurley, L.H. DNA and its associated processes as targets for cancer therapy. *Nat. Rev. Cancer* **2002**, *2*, 188-200.

(69) Rohs, R.; Jin, X.; West, S.M.; Joshi, R.; Honig, B.; Mann, R.S. Origins of Specificity in Protein-DNA Recognition. *Annu. Rev. Biochem* **2010**, *79*, 233-269.

(70) Cadet, J.; Davies, K.J.A. Oxidative DNA damage & repair: An introduction. *Free Radical Biol. Med.* **2017**, *107*, 2-12.

(71) Rothbart, S.B.; Strahl, B.D. Interpreting the language of histone and DNA modifications. *Biochim. Biophys. Acta, Gene Regul. Mech.* **2014**, *1839*, 627-643.

(72) Jing, M.; Bowser, M.T. Methods for measuring aptamer-protein equilibria: A review. *Anal. Chim. Acta* **2011**, *686*, 9-18.

TOC GRAPHIC

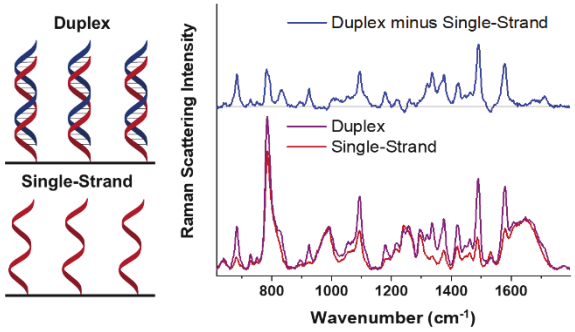
Duplex
Single-Strand
Raman Scattering Intensity
Duplex minus Single-Strand
Duplex
Single-Strand
800
1000
1200
1400
1600
Wavenumber (cm-1)